



Funded by the Seventh Framework
Programme of the European Union



Project full title:
Hepatic and Cardiac Toxicity Systems modelling

Project acronym:
HeCaTos

Collaborative project
HEALTH.2013.1.3.-1:
Modelling toxic response in case studies for predictive human safety assessment

FP7-HEALTH-2013-INNOVATION-1-602156-HeCaTos

Deliverable Report D3.3:
**Report on multi-scale models integrating cellular toxicity pathways
into cardiac and hepatic cell types**

Work package 3
Due date of deliverable: M40
Actual submission date: M41

Start date of project: October, 2013

Duration: 60 months

Maastricht University (UM)

Project co-funded by the European Commission within the 7th Framework Programme (2013-2018)		
Dissemination Level		
PU	Public	X
PP	Restricted to other programme participants (including the Commission Services)	
RE	Restricted to a group specified by the consortium (including the Commission	
CO	Confidential, only for members of the consortium (including the Commission Services)	

Contributions to deliverable - Internal review procedure

Deliverable produced by:	Date:
Alex Lewalle - Partner ICL	January 2017
Steven Niederer - Partner ICL	January 2017
Lars Oliver K�pfer - Partner RWTH AACHEN	January 2017
Deliverable internally reviewed by:	Date:
Jos Kleinjans - Partner UM	February 2017

Contents

Publishable Summary.....	3
Objectives	3
Introduction - Workflow overview.....	3
General model development	4
Inclusion of HeCaToS data within the model.....	6
Anatomical dimensions and pressure.....	6
Proteomics analyses	8
Implementation of measurements into the model	10
Results.....	11
Outlook	12
Drug-induced liver injury	15
PBPK-based contextualisation of <i>in vitro</i> toxicity data (PICD)	15
Multiscale modelling of mitochondrial dysfunction	16
References	21

Publishable Summary

We developed a multi-scale computational model framework for simulating heart contraction. The model is sufficiently detailed to include the main known aspects of cardiac muscle behaviour, while retaining enough simplicity to enable parameterisation using standard clinical measurements. Further, we aim to exploit this flexibility to simulate the effect of anthracycline treatment (through the alteration of relevant model parameters), and hence to shed light onto the predominant mechanistic underpinning of observed clinical responses to drug treatments.

With regard to modelling of drug-induced hepatotoxicity, physiology-based pharmacokinetic (PBPK) modelling was used to simulate concentration profiles in the interstitial compartment of the liver which were in turn used as an extracellular input signal for the cellular network. This approach has been used for the PBPK-based contextualisation of in vitro toxicity data (PICD, Thiel et al., 2016) and for the development of multiscale models describing cases of mitochondrial dysfunction in metabolic network models.

Objectives

We seek to gain insight into the physiological basis underlying anthracycline cardiotoxicity by analysing the different constitutive mechanisms of the heart by computational modelling. The model aims to reproduce directly measurable cardiac behaviour, as acquired from anthracycline-treated patients. For this purpose, the left-ventricular ejection fraction (LVEF), a metric of cardiac function routinely measured in clinical settings, provides a convenient benchmark for comparisons of the cardiotoxic and healthy hearts. Echocardiography measurements, performed both on anthracycline-treated patients and on a control cohort, indicate a significant decrease (from ~60% to 30% on average) in the LVEF, several months following the drug treatment. Proteomics studies (performed within the HeCaToS project) also suggest a change in the abundance of proteins that participate in the cardiac contraction mechanism, as a result of anthracycline application to pluripotent human cardiac myocyte stem cells. Combining these measurements, our computational model provides a framework for exploring cardiac function from a mechanistic perspective, and for comparing, quantitatively, the relative significance of the different mechanistic and structural contributions to observed cardiac function, ranging from organ-scale anatomical remodelling to sub-cellular protein interactions.

Drug-induced toxicity caused by extensive drug exposure is a significant problem in clinical care. Understanding the molecular mechanisms accompanying the transition from desired drug effects to adverse events following administration of therapeutic and toxic doses is still missing, in particular at patient level. By integrating cellular pathway information into physiologically-based pharmacokinetic models time-resolved drug responses at patient level could be described. Comparatively studying toxic changes across the considered hepatotoxins allows the identification of subsets of drugs sharing similar perturbations on key cellular processes, functional classes of genes, and individual genes. The results may facilitate the early diagnosis of adverse drug events in clinical application.

Introduction - Workflow overview

Our analysis workflow is summarised in Figure 1. In the first step, a generic finite-element mesh template is generated. This template is then parameterised using available measurements (either obtained within the HeCaToS project, or by using literature values), to give a “baseline” model that reproduces the cardiac function of a typical healthy heart. Starting from this baseline model, we can

assess the sensitivity of various clinical phenotypes to individual mechanistic model parameters, in particular, those parameters that have been identified as showing a significant affected by anthracycline exposure. The framework thus serves as a virtual laboratory for investigating drug effect on the separate cardiac subsystems, and the resulting impact on global cardiac function.

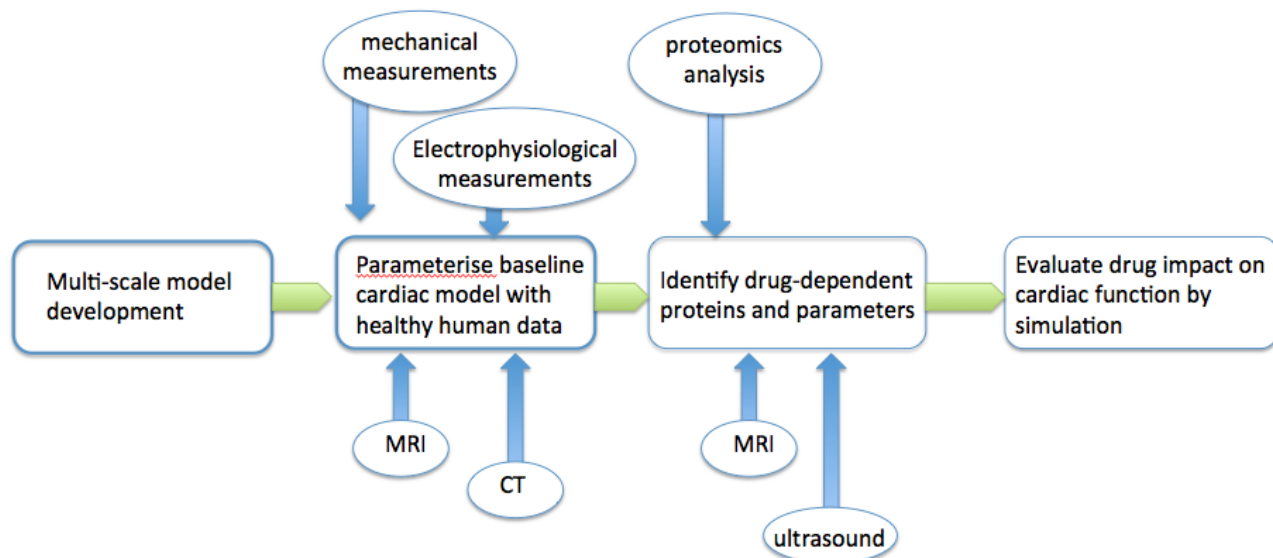


Figure 1: Outline of the modelling workflow, integrating imaging measurements and proteomics analyses into the finite-element computational model.

General model development

The multi-scale model framework, outlined in Figure 2, encompasses cardiac properties ranging from the cellular level (myocyte mechanical and electrophysiological behaviour) to the whole heart.

The passive elastic and active contractile contributions to the tissue mechanics are expressed in relation to predefined muscle-fibre orientations. Following common practice, the mechanical properties are assumed to display transverse isotropic symmetry with respect to the muscle fibre coordinate system.

Contractile forces are exerted along the fibre directions following stimulation by an externally imposed calcium signal. The mechanistic model that generates tension from this signal mimics the binding of calcium to troponin C, which in turn allows the formation of tension-generating myosin crossbridges. The implementation of this protein-level mechanism within our framework provides a handle for including the drug-induced proteomics analyses available in the HeCaToS project.

The model aims to reproduce the principal observable features of the cardiac cycle under physiological conditions. As described in the following sections, the model parameters that govern tension generation and the mechanical response can be constrained either using direct measurements or literature data. The resulting model provides a setting for investigating cardiac function with maximum consistency, in particular by assessing the impact of specific parameters that are altered by drug exposure.

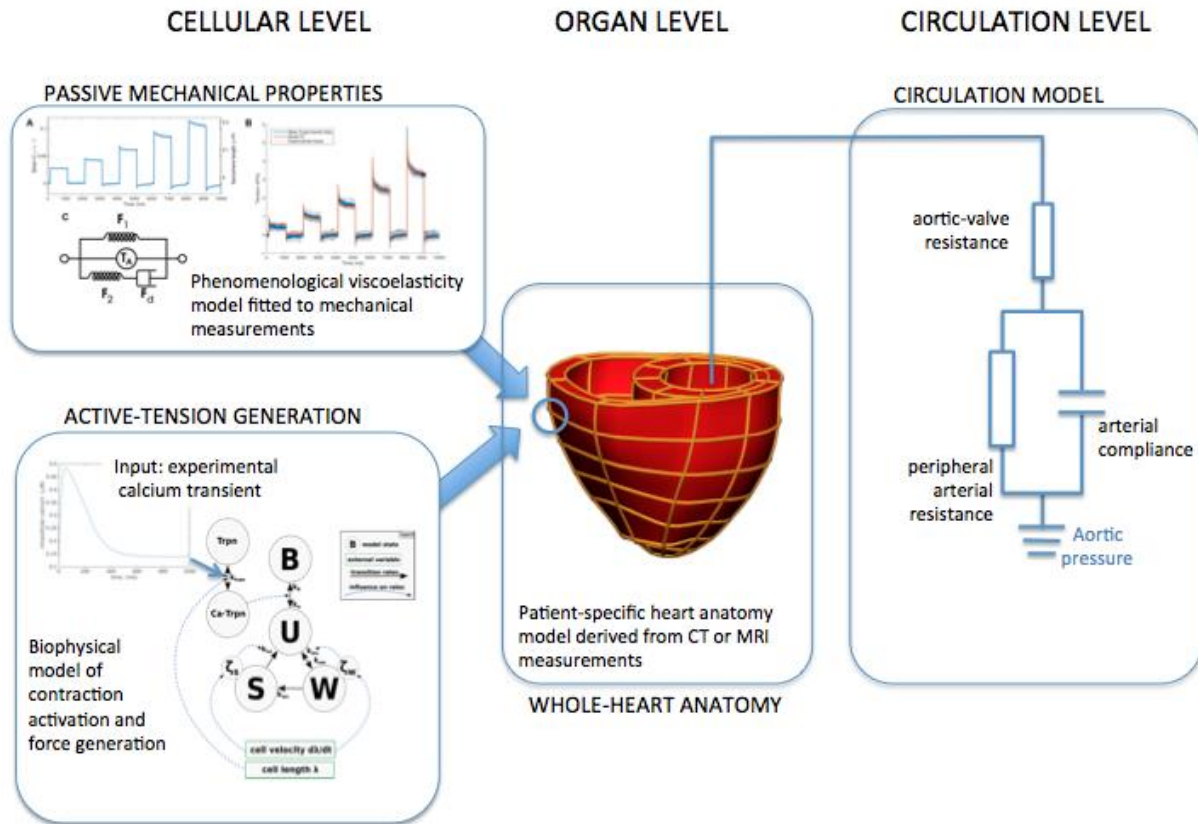


Figure 2: General model structure. The tissue is modelled as a viscoelastic material with both passive and active properties. During contraction, blood volume is ejected from the left ventricle to the body circulation, modelled as a "Windkessel" system

Figure 3 shows the output of a typical simulation. The contraction/relaxation cycle of the left ventricle is reproduced. Its four main phases allow a direct comparison with clinical measurements.

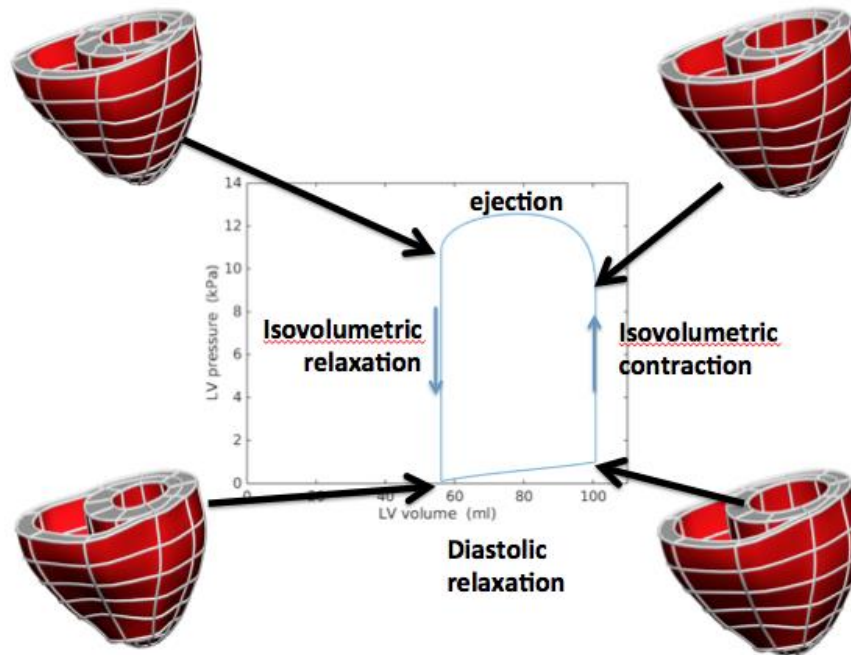


Figure 3: Typical outcome of the contraction simulation. The four principal phases of the contraction-relaxation cycle are reproduced, allowing a direct matching to measurements.

Inclusion of HeCaToS data within the model

Anatomical dimensions and pressure

The data sources used for calibrating the model geometry include echocardiography and pressure measurements. For simplicity, these data were used to define a minimal set of phenotypes, to characterise the heart function in terms of three metrics that are readily measurable in a clinical setting: the LV end-diastolic diameter (LVEDD), the maximum ejection pressure (MEP) and the LVEF. In the absence of relevant experimental or clinical measurements, details of the cardiac cycle relating to the diastolic relaxation phase are neglected for the present purpose.

The histograms in Figure 4 show the distribution of cardiac measurements in healthy control and doxorubicin-treated patients, constructed from the echocardiography data provided by Jort Merken for HeCaToS: the LVEDD, the thicknesses of the interventricular septum (IVS) and the left-ventricular posterior wall (LVPW), the MEP and the LVEF (the treated patient cohort includes patients who were treated with doxorubicin only). The average measurements for the control and treated cohorts are compared in the table.

The clearest difference between the two cohorts is in the LVEF, which is significantly greater in the control population (~60%) than in the treated patients (~30%, albeit with one outlier with an LVEF of 64%). In contrast, the results suggest no noticeable alteration in the LV wall thicknesses. A small increase in the LVEDD (from ~47 mm in the controls to ~60 mm in the doxorubicin patients) and a small decrease in MEP (from 19 to 16 kPa) are observed.

One question that we will therefore seek to answer is whether the observed small difference in LVEDD distributions can, by itself, account quantitatively for the very large difference in LVEF, i.e., whether cellular-level changes must be invoked to explain this difference.

PATIENT	SEX	AGE	TREATMENT
10027	F	65	Epirubicin, doxorubicin, tamoxifen
10132	F	82	Epirubicin, docetaxel
10188	F	51	cyclophosphamide
10201	F	56	Adriamycine, cyclophosphamide, taxotene, everolimus, exemestane
10204	F	68	Cyclophosphamide, letrozol, radical radiotherapy
10206	M	53	Doxorubicin, cyclophosphamide, vincristine, prednison
281	M	44	5-FU, cetuximab, carboplatin
442	F	69	Doxorubicin, +extra
501	M	55	Cisplatin, pemetrexed
614	F	65	Cyclophosphamide, doxorubicin, 5-Fluorouracil (5-FU)
708	M	36	Control
731	F	58	Doxorubicin 5-FU, cyclophosfamide
742	M	53	Control
744	M	53	Control
842	M	62	Sandostatine

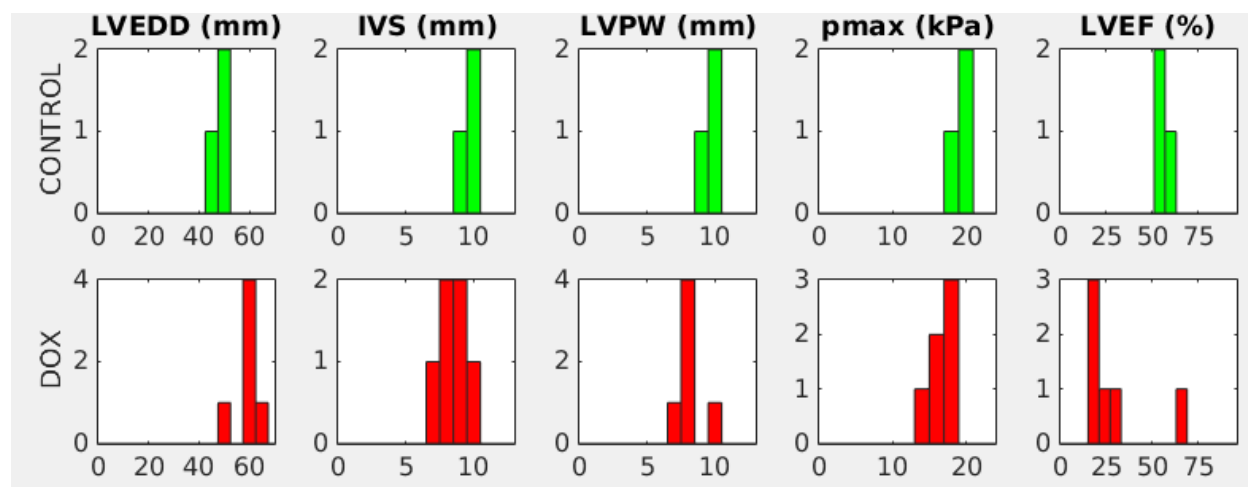


Figure 4: Histograms of phenotype measurements: left ventricular end-diastolic diameter (LVEDD), interventricular septum (IVS) and posterior wall (LVPW) thicknesses, maximum ejection pressure (pmax), and ejection fraction (LVEF) for healthy controls and doxorubicin-treated patients

Table 1: Summary of distribution values (Figure 4 histograms)

Measurement	mean value	std
LVEDD (mm) CONTROL	47	3
LVEDD (mm) DOX	60	5
IVS (mm) CONTROL	10	1
IVS (mm) DOX	8	1
LVPW (mm) CONTROL	10	1
LVPW (mm) DOX	8	1
MEP (kPa) CONTROL	19	1
MEP (kPa) DOX	16	2
LVEF (%) CONTROL	58	1
LVEF (%) DOX	31	

Proteomics analyses

The proteomics analyses carried out within the HeCaToS project allow a quantification of protein abundances, in the presence or absence of anthracycline treatment, by mass spectrometry. The datasets made available within the HeCaToS project are derived from different sources. One dataset was obtained from *in vitro* preparations of pluripotent human cardiac myocyte stem cells subjected to a two-week anthracycline exposure protocol. A second dataset was derived from biopsy samples. Both datasets aim to allow a comparison of a “cardiotoxic” state with controls.

Data spreadsheets, provided for HeCaToS by Hans Gmünder, were searched for the proteins that play a direct role in the cardiac contraction process. Table 2 summarises the results for the main proteins of interest, based on the “two-week stem-cell” dataset.

We note the particularly significant impact of doxorubicin on those proteins that regulate myosin crossbridge formation in the myocytes: troponins C, I and T, and tropomyosin. As an example, Figure 5 shows the time dependences of the troponin C abundances (normalised to the initial value at the start of the treatment). To compare the relative effect of the drug on all the proteins in the dataset, Figure 6 plots the mean rates of change in protein abundances for the therapeutic and toxic treatments. The points representing the troponins and tropomyosin are clear outliers in the overall distribution, which suggests that they are particularly strongly affected by doxorubicin treatments, at least for the higher dose.

PROTEIN	PROTEIN CODE	EFFECT OF DOXORUBICIN OVER 14 DAYS
Sodium-potassium pump (alpha 1)	AT1A1_HUMAN	No systematic effect above noise level
Sodium-potassium pump (alpha 2)	AT1B1_HUMAN	No systematic effect above noise level
SERCA	AT2A2_HUMAN	No systematic effect above noise level
Calcium pump	AT2B4_HUMAN	No systematic effect above noise level
Calmodulin	CALM_HUMAN	Decrease by ~20% at both therapeutic and toxic doses
Phospholamban	PPLA_HUMAN	No systematic effect above noise level
Sodium-calcium exchanger	NAC1_HUMAN	No systematic effect above noise level
Titin	TITIN_HUMAN	Increase by ~60% at toxic dose
Troponin C	TNNC1_HUMAN	No effect at therapeutic dose; 70% decrease at toxic dose
Troponin I	TNNI3_HUMAN	~50% decrease at therapeutic dose; ~70% at toxic dos
Troponin T	TNNT2_HUMAN	No effect at therapeutic dose; ~70% decrease at toxic dose
Tropomyosin alpha-1 chain	TPM1_HUMAN	No effect at therapeutic dose; ~80% decrease at toxic dose
Tropomyosin beta chain	TPM2_HUMAN	No effect at therapeutic dose; ~70% decrease at toxic dose
Tropomyosin alpha-3 chain	TPM3_HUMAN	Inconclusive

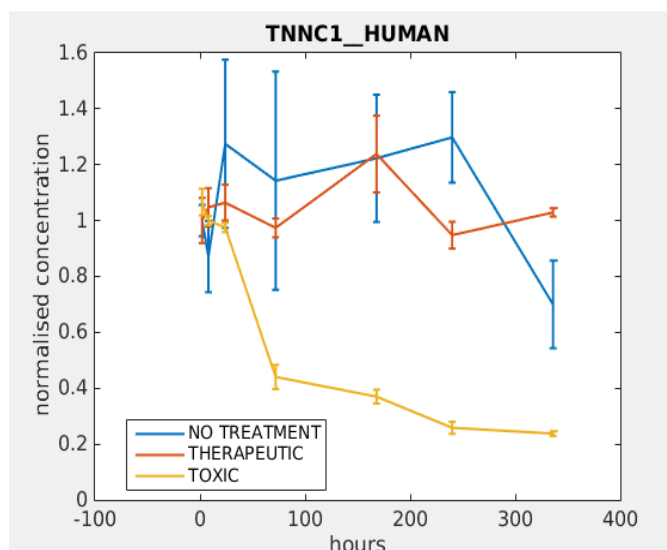


Figure 5: Time dependence of troponin C abundance (normalised to initial value) in untreated myocytes and myocytes treated with therapeutic and toxic doses of doxorubicin

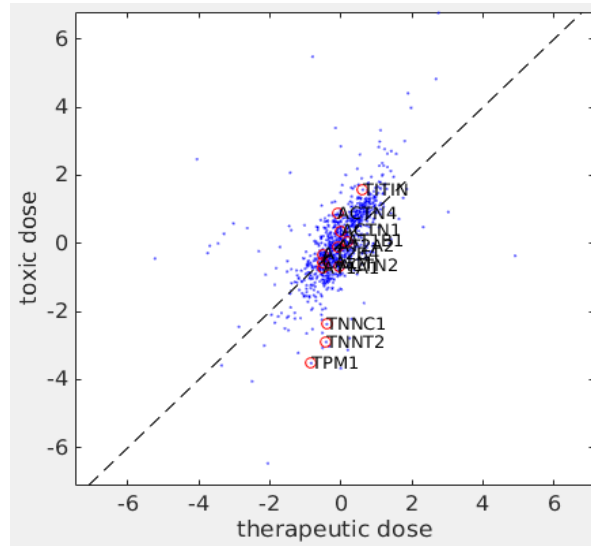


Figure 6: Overview of the complete proteomic dataset, showing the average rates of change of individual proteins under therapeutic and toxic doses. The troponins and tropomyosin show significant dox dependence for toxic doses.

Implementation of measurements into the model

The implementation of the clinical and experimental results described above follows the flowchart in Figure 1.

The first step is to design an appropriate geometrical finite-element mesh, based on the geometrical measurements. The echo measurements reported above identified a significant correlation between the LVEDD and the LVEF, while the wall thickness seemed to be unchanged by doxorubicin. To include this LVEDD dependence of cardiac behaviour, we constructed ellipsoidal meshes of varying diameter and constant wall thickness and length (Figure 7). By using these meshes as generalised representations of the left ventricle, instead of meshes based directly on real heart segmentations, we seek to achieve a more objective assessment of the LVEDD significance specifically, independently of the other model parameters.

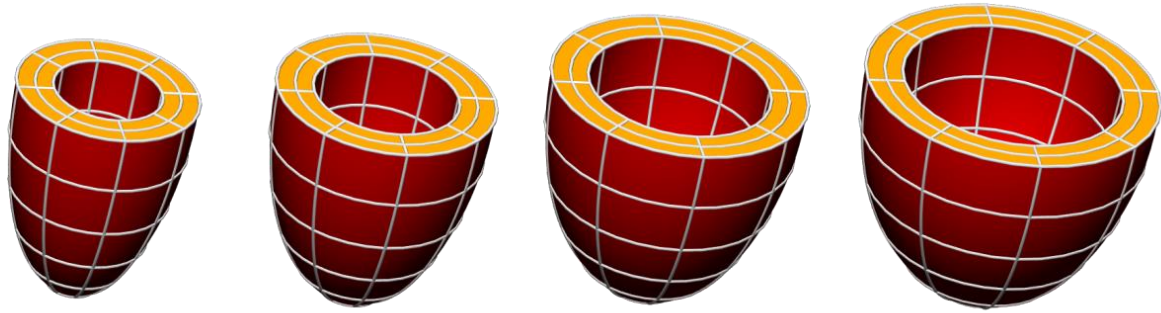


Figure 7: Hypothetical ellipsoidal meshes representing the left ventricle, with diameters of 15, 20, 25 or 30 mm, wall thickness 10 mm, and apex-base distance 65 mm.

Simulations were performed using the above meshes and the theoretical contraction model described by Sand et al. (2016), the most up-to-date model available focusing specifically on the human heart. Its baseline parameterisation characterises both passive and viscoelastic properties, as well as static and dynamic active-force generation, based on measurements in skinned human cardiac myocytes. The model parameters were fine-tuned in order to reproduce the phenotypes of the “control” cohort (green histograms in Figure 4).

Results

Figure 8 plots the dependences of the simulation outputs (LVEDD, MEP, and EF) as functions of the tissue stiffness for different values of the reference-mesh inner radius (r_{endo}). The results highlight the strong dependence of both LVEDD and EF on r_{endo} . The decrease in EF with increasing r_{endo} , with all other parameters kept constant, follows the trend observed in the histograms of Figure 4.

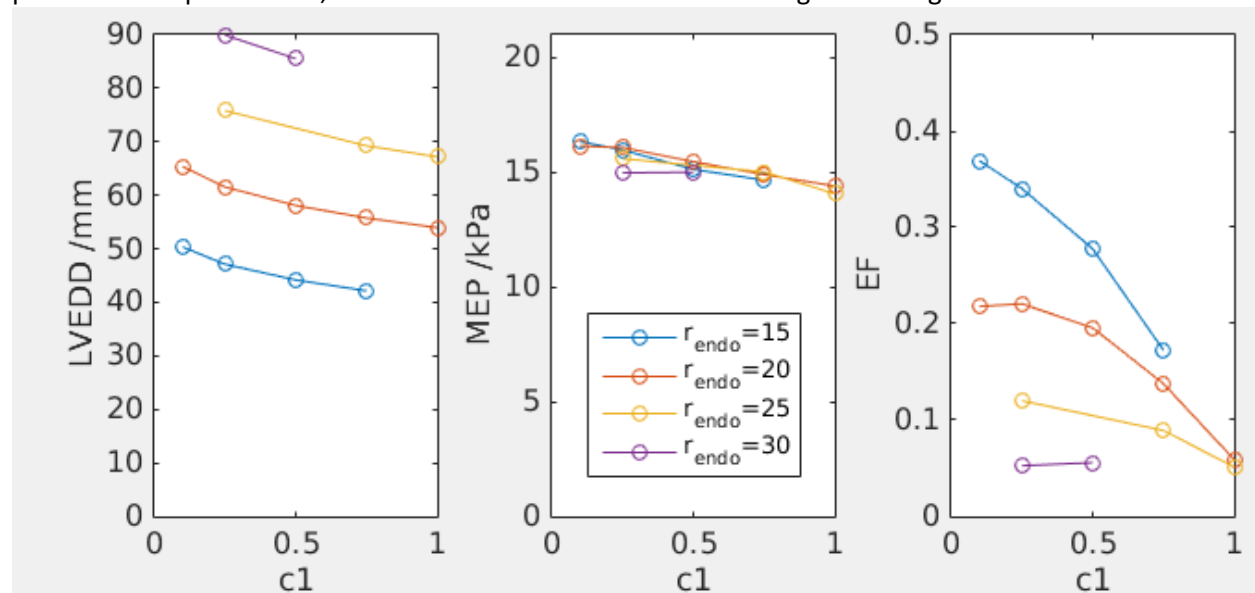


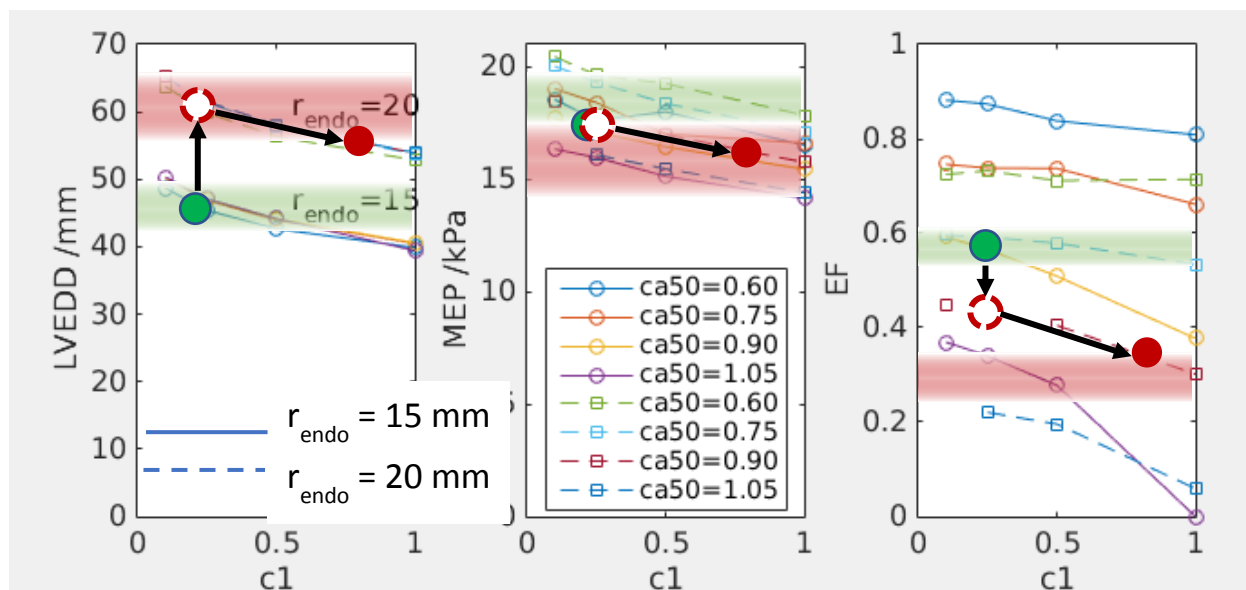
Figure 8: Simulation outputs as a function of the tissue stiffness $c1$, for different values of the reference-mesh inner radius (r_{endo})

An important question is to what extent the geometrical broadening of the left ventricle can account for the full decrease in EF. To address this question, Figures 9, 10, and 11 consider the combined effects, on the simulation results, of changing various parameters in addition to *rendo*. We consider variations in three different parameters: *c1* (the tissue stiffness), *Tref* (the maximal muscle tension expected, in the model, when the muscle fibres are at their resting length) and *maxTnC* (the relative concentration of troponin C proteins). The premise of this analysis is that each set of model parameters yields a set of simulation outputs that can be compared for consistency with the clinical parameters (the histograms of Figure 4 and Table 1). To facilitate this comparison graphically, we denote the expected range of clinical values with green- or red-shaded horizontal bars in the simulation output plots.

Starting from one particular set of simulation parameters that is consistent with the “control” distributions of outputs (i.e., producing green dots that are located within each of the green-shaded regions), we see that increasing *rendo* from 15 to 20 mm (the transition leading from the green dot to the white dot) achieves satisfactory agreement with the measured doxorubicin LVEDD. However, the corresponding decrease in EF is too small to achieve consistency with the doxorubicin distribution (i.e., the white dot is located significantly far away from the horizontal red range). By changing either *c1* (in Figure 9), *Tref* (Figure 10), or *maxTnC* (Figure 11), full consistency is achieved more satisfactorily, with the red dot lying in all three horizontal red ranges.

Outlook

The three examples of different possible “trajectories” (Figures 9, 10 & 11), linking the healthy heart to the heart suffering from doxorubicin cardiotoxicity, highlight the complexity of the interacting subsystems in the heart. Our ongoing work continues to explore the parameter space around these trajectories. Our goal in this process is to use the available measured data to impose bounds on the modelling parameters, in order to clarify the most likely dominant physiological pathways that underlie cardiotoxicity.



- = healthy control
- = intermediary state
- = cardiotoxic state

Figure 9: Simulation outputs plotted as functions of tissue stiffness $c1$, for different values of the troponin C calcium sensitivity and for two reference-mesh radii, $r_{\text{endo}} = 15$ and 20 mm. The horizontal green and red bars indicate, respectively, the control and doxorubicin-treated distributions specified by the clinical measurements (Figure 4, Table 1). The green, white and red dots indicate a “trajectory” in the model phase space whereby the heart can evolve from the “control” to the “doxorubicin” distribution through the combination of the r_{endo} and $c1$ parameters.

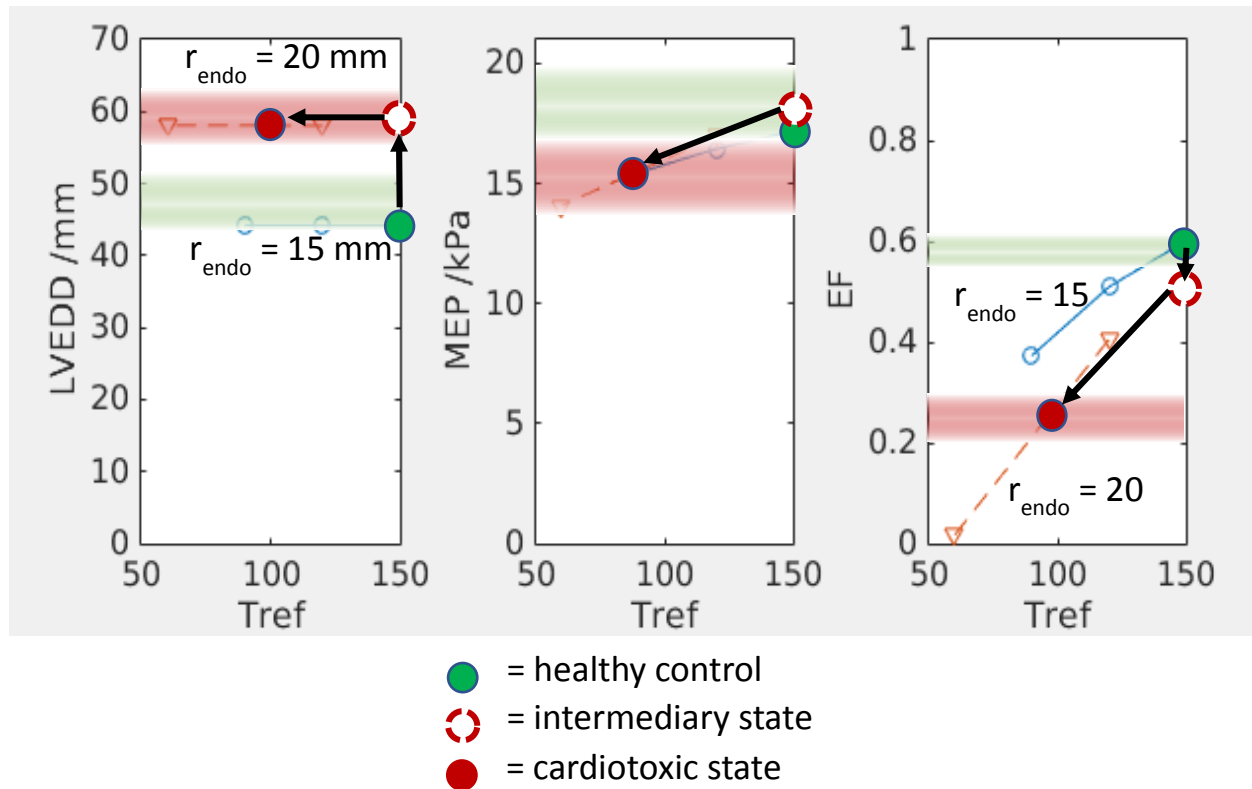


Figure 10: Simulation outputs plotted as functions of the muscle maximum resting-length tension T_{ref} , for the two reference-mesh radii, $r_{endo} = 15$ and 20 mm. The green, white and red dots indicate a “trajectory” in the model phase space whereby the heart can evolve from the “control” to the “doxorubicin” distribution through the combination of the r_{endo} and T_{ref} parameters.

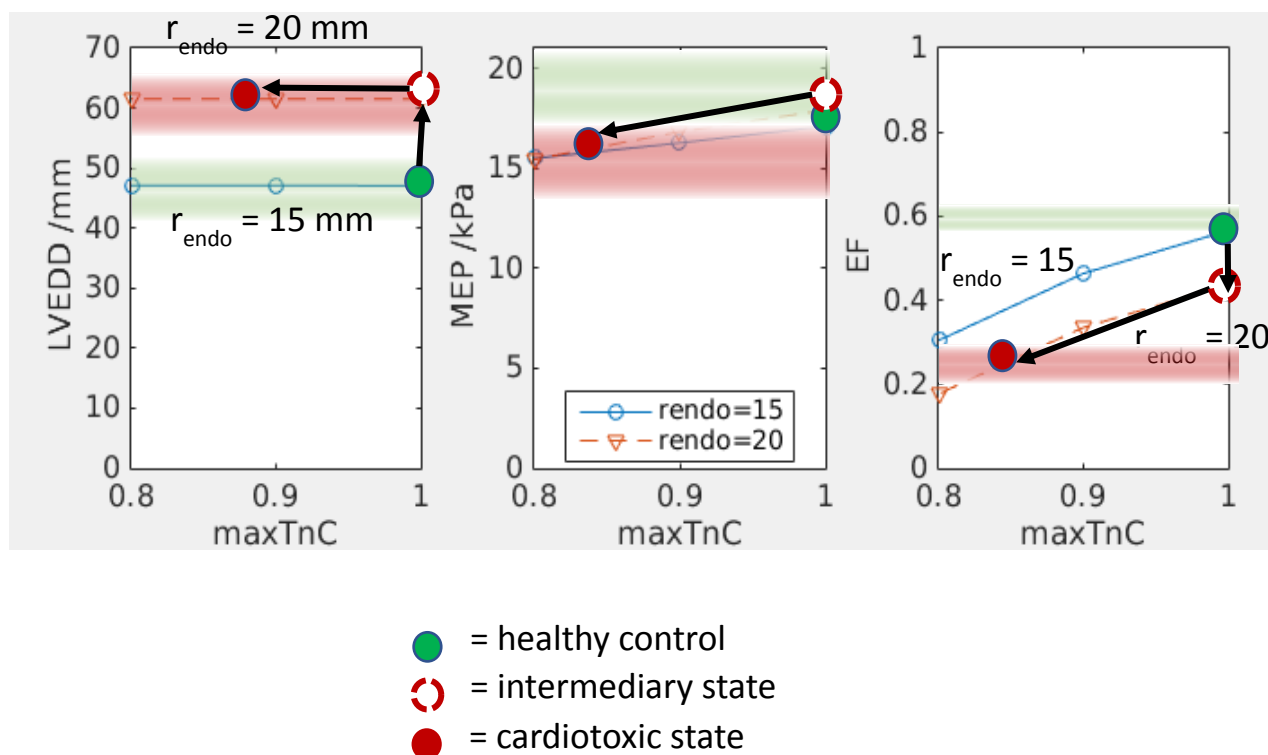


Figure 11: Simulation outputs plotted as functions of the relative troponin C concentration, for the two reference-mesh radii, $r_{\text{endo}} = 15$ and 20 mm. The green, white and red dots indicate a “trajectory” in the model phase space whereby the heart can evolve from the “control” to the “doxorubicin” distribution through the combination of the r_{endo} and maxTnC parameters.

Drug-induced liver injury

Physiology-based pharmacokinetic (PBPK) modelling was used to simulate concentration profiles in the interstitial compartment of the liver for the analysis of drug-induced hepatotoxicity. The simulated concentration profiles were in turn used as an extracellular input signal for the cellular network models. This approach has been used for the PBPK-based contextualisation of *in vitro* toxicity data (PICD, Thiel et al., 2016; Thiel et al., 2017a; Thiel et al., 2017b) and for the development of multiscale models describing cases of mitochondrial dysfunction in metabolic network models.

PBPK-based contextualisation of *in vitro* toxicity data (PICD)

In vitro toxicity data from the Open TG-GATEs library (Igarashi et al. 2015) were exemplarily integrated into drug-specific whole-body PBPK models to translate drug-induced *in vitro* findings to an actual *in vivo* situation (Figure 12). PICD thus allows the establishment of drug-specific dose-response correlations. In particular, cellular pathway responses can be analysed within an *in vivo* context. This will be illustrated in the following for an analysis of the effect of azathioprine (AZA) and valporic acid (VPA) on cell cycle checkpoint regulation (Thiel et al., 2017a).

In a comparative study of 15 hepatotoxicants, functional classes of genes were identified which showed similar toxic behavior of AZA and VPA in the regulation of the cell cycle G2/M DNA damage checkpoint despite a significant pharmaceutical and chemical diversity (Thiel et al., 2017a). The G2/M DNA damage checkpoint represents the second checkpoint in the cell cycle and ensures that genomic stability is

maintained by repairing damaged DNA before entering the mitosis phase (Figure 14A) (Löbrich & Jeggo, 2007). This pathway is hence crucially involved in DNA replication, recombination, and repair, respectively and is consequently essential for cell viability (Kastan & Bartek, 2004). A key role for the transition from the G2 phase to the M phase forms the cyclin-dependent kinases and several transcription regulators (Figure 14A) (Nigg, 1995).

To directly compare the toxic behavior between both drugs, the differences of toxic change were calculated for all involved genes (Figure 14B). Analyzing differences in toxic changes revealed similar effects at 2h for several genes (Figure 14B). Only the p53 regulator MDM4, and the phosphatase PPM1D, the kinases CKS2 and CDC2 as well as the stress sensor GADD45, demonstrated high differences of toxic change for VPA and AZA, respectively (Figure 14B).

The differentially responding genes were next used to build differential response pathways at given timepoints (Figure 14C, D, E & F). Exploring these pathways helps to compare dynamic changes between AZA and VPA in the regulation of the cell cycle G2/M DNA damage checkpoint when switching from therapeutic to toxic dose administration.

Analyzing differential response pathways of AZA at 2h (Figure 14C) and VPA at 8h (Figure 14E) revealed that AZA highly perturbed GADD45 and CKS2, which regulates CDC2-cyclin B complex, while VPA affected the same key complex by strongly perturbing p53 via HIPK2, on the one hand, and p90RSK, Myt1, and CDK7, on the other hand. Interestingly, GADD45 and CKS2 were involved in both pathways but in a time-shifted manner. In order to regulate key processes of the cell cycle G2/M checkpoint at 24h, BORA and DNA-PK were highly affected by AZA (Figure 14D). In contrast, a significantly higher activity due to VPA administration was observed at the same timepoint thereby regulating all major processes mostly via p53, MDM2 and CDC2 (Figure 14F). The presented analysis is an illustrative example, how PICD can be used to establish dose-response-correlations at the pathway level and hence foster comprehensive analyses of cellular responses in the light of extracellular stimuli.

Multiscale modelling of mitochondrial dysfunction

In a second approach we developed a generic workflow that combines dynamic drug pharmacokinetics represented by compound and patient specific PBPK models with genome scale metabolic network models (**Error! Reference source not found.**⁵**Error! Reference source not found.**). In particular, the resulting multiscale model quantifies the impact of drug exposure on endogenous metabolism. The applicability for this workflow was shown for various classes of drugs, including an analgesic (acetaminophen), an antibacterial (isoniazid) and an anticonvulsant (Valproic acid) compound.

PBPK models of APAP, INH and VPA were first established by using literature PK data. The PBPK models were linked to the cellular network models by coupling the interstitial space of the liver to the metabolic network model. Notably, the intracellular enzymatic reaction rates estimated in the PBPK model directly correspond to the intercellular reaction rates in the represented analogously in the cellular network (Fig. 15). This allows to mechanistically quantify drug induced metabolic changes on the cellular metabolism of the liver in a time-resolved manner. Accumulated flux changes in metabolic network were quantified for APAP, VPA and INH and cellular subsystems which were affected were identified (Figure 15). This approach will be further improved in the future and compared to clinical and experimental toxicity data.

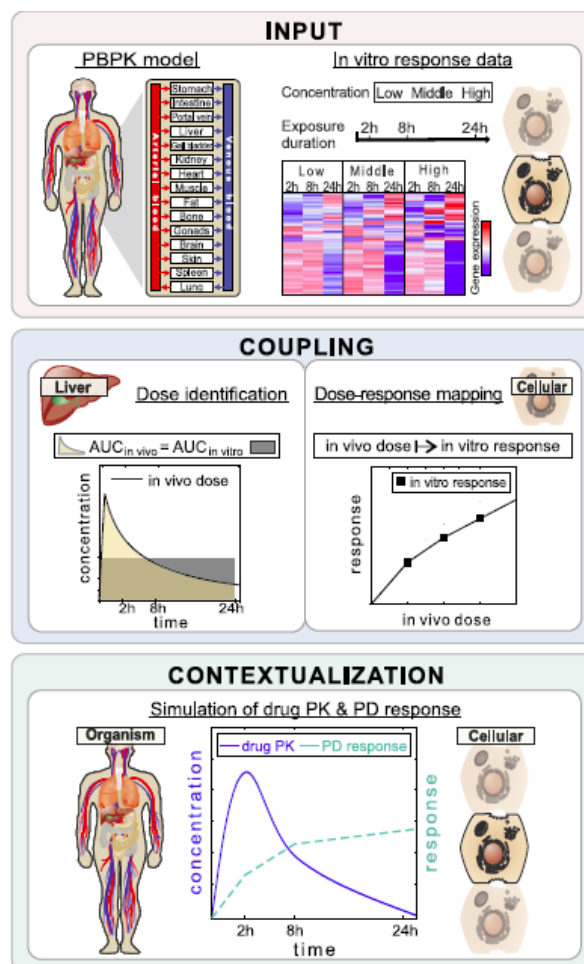


Figure 12: PBPK-based *in vivo* contextualization of *in vitro* toxicity data (PICD).

INPUT: At the organism level, PBPK models are developed for specific drugs. At the cellular level, *in vitro* response data of compound-treated primary hepatocytes are analyzed. **COUPLING:** *In vivo* doses are identified, which are directly related to *in vitro* drug exposure ($AUC_{in\ vivo} = AUC_{in\ vitro}$). Time-dependent dose-response curves are built by mapping *in vivo* doses to *in vitro* responses. **CONTEXTUALIZATION:** By use of the time-dependent dose-response curves drug responses over time are predicted for PK profiles simulated for different doses.

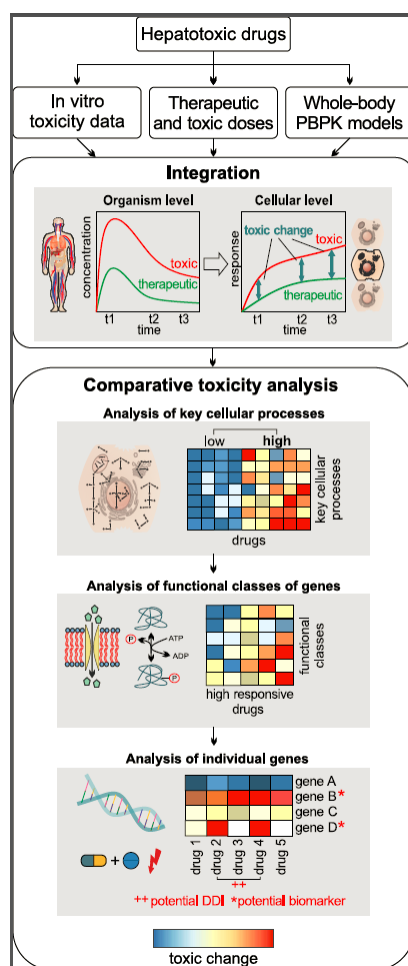


Figure 13: Consideration of therapeutic and toxic doses within a whole-body PBPK context. For a set of hepatotoxic drugs, toxic changes will be measured at different timepoints (2h, 8h, 24h) by comparing cellular response following drug administration of therapeutic and toxic doses and will be subsequently evaluated with regard to key cellular processes, functional classes of genes, and individual genes, respectively (Thiel et al, 2017a).

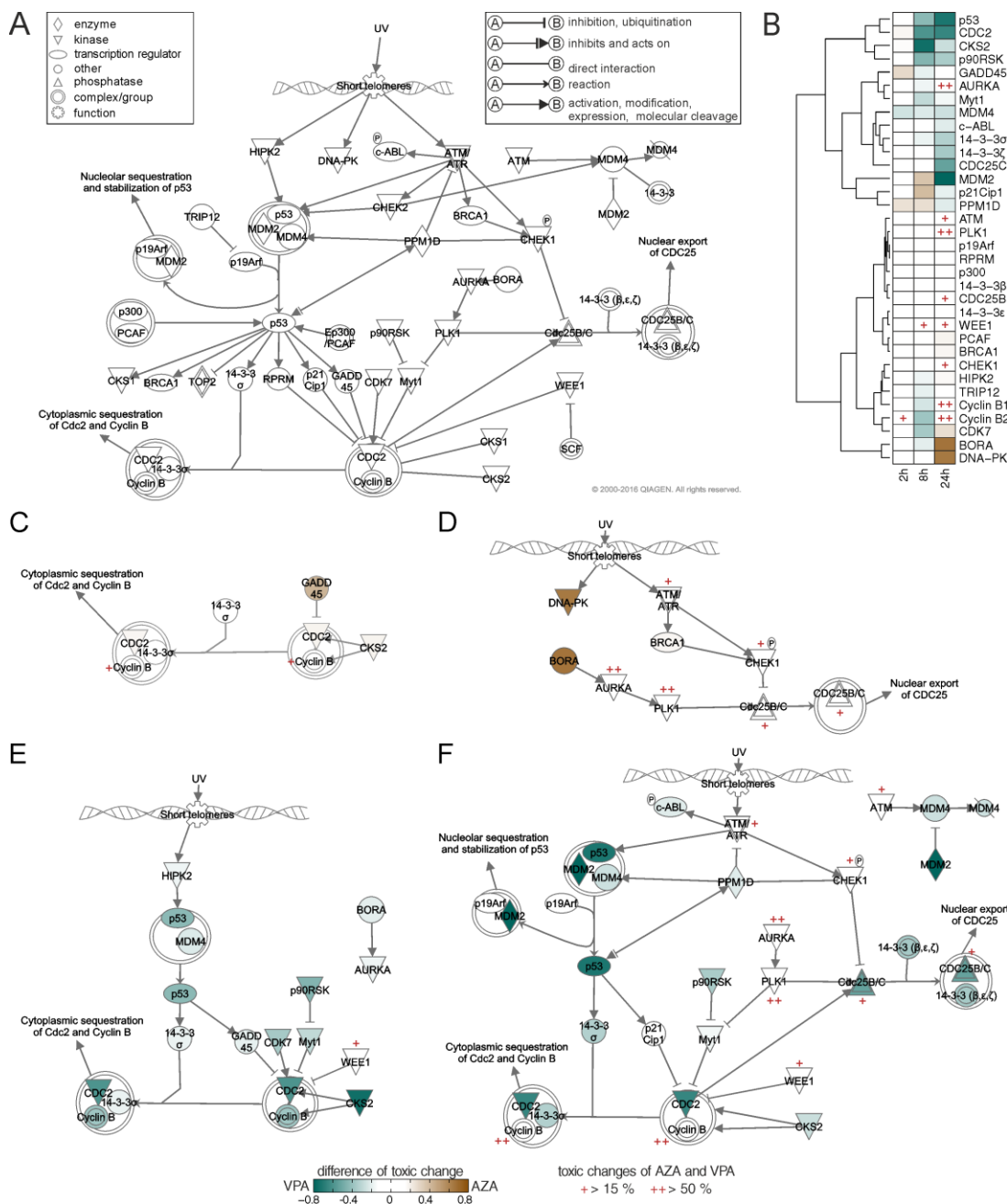


Figure 14: Comparison of toxic changes between AZA and VPA and differential response pathways at different timepoints:

A) Pathway of 'cell cycle G2/M DNA damage checkpoint regulation';

B) Comparison of toxic changes for involved genes between AZA and VPA;

C) AZA, 2h;

D) AZA, 24h;

E) VPA, 8h;

F) VPA, 24h.

The colorbar depicts differences of toxic changes between both drugs. Genes with high toxic changes for both drugs were explicitly marked in red.

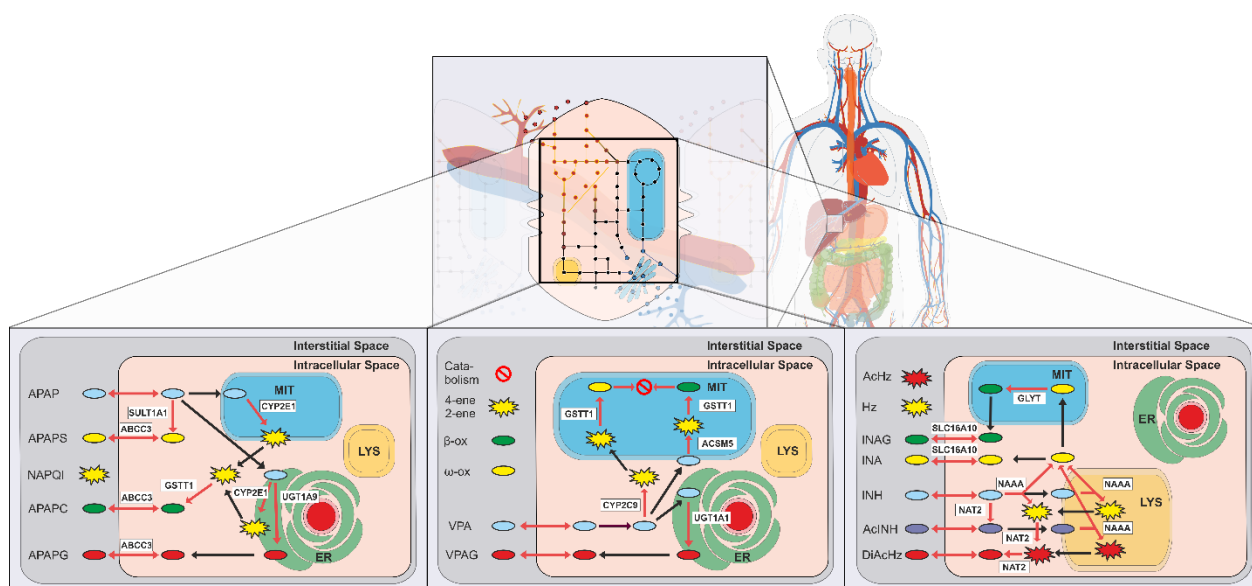


Figure 15: Integration of drug metabolic reactions into tissue specific genome scale metabolic network models. Black arrows are reactions which do not interfere with the host metabolism, red arrows indicate consumption or production of endogenous metabolites. Oval shapes are metabolites cleared from the body via catabolism of urinary excretion, stars are toxic compounds being formed during xenobiotic metabolism.

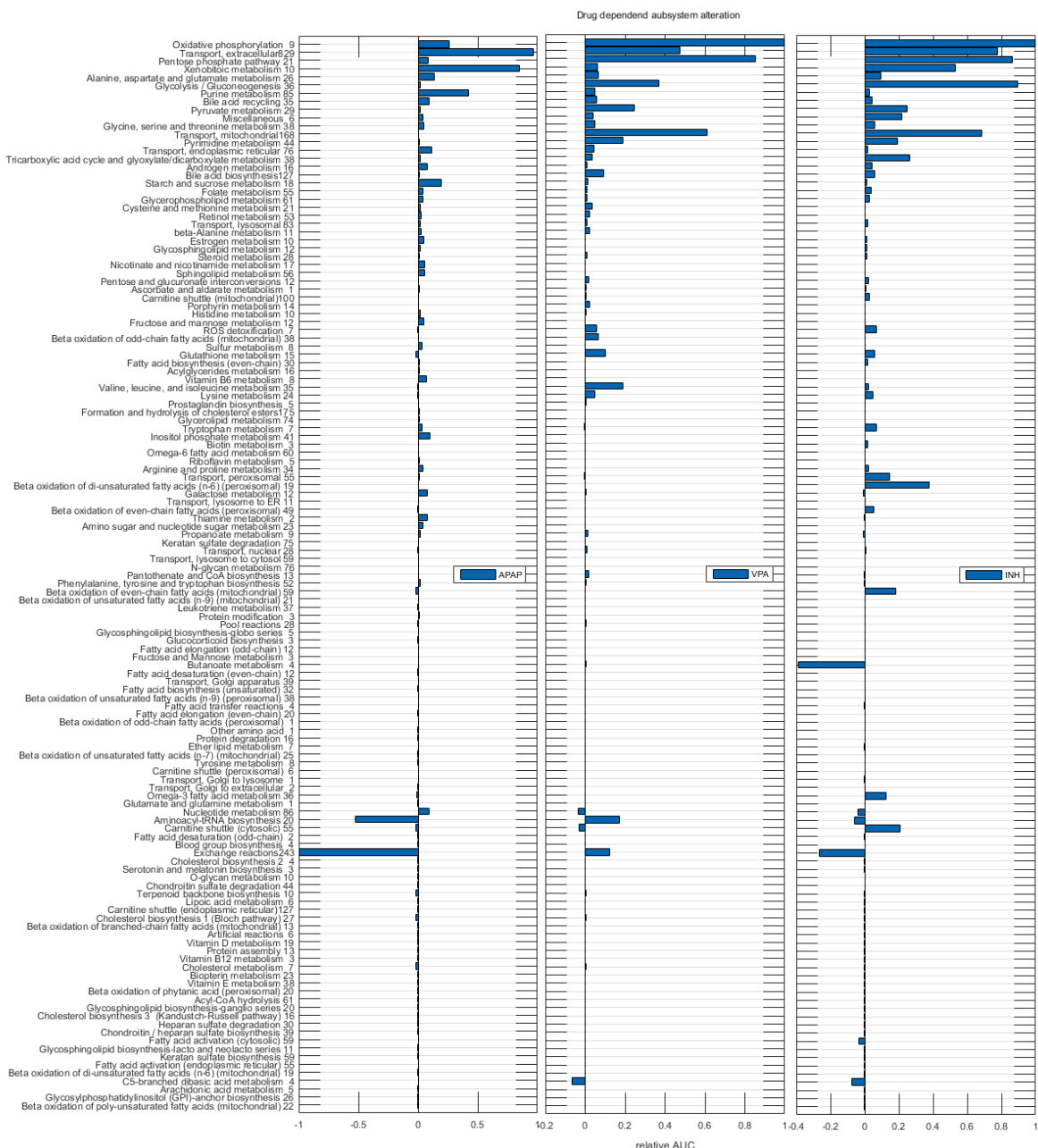


Figure 16: Cellular subsystems ranked based on integrated flux alterations after drug perturbation.

References

- Land et al., An analysis of deformation dependent electromechanical coupling in the mouse heart, *J. Physiol.*, 590(18), 4553 (2012).
- Land et al., *A model of cardiac contraction based on novel measurements of tension development in human cardiomyocytes*, submitted (2016).
- Thiel C, Cordes H, Conde I, Castell JV, Blank LM, Kuepfer L. Model-based contextualization of in vitro toxicity data quantitatively predicts in vivo drug response in patients. *Arch Toxicol.* 2016.

- Thiel C, Cordes H, Baier V, Blank LM, Kuepfer L. Multiscale modeling reveals inhibitory and stimulatory effects of caffeine on acetaminophen-induced toxicity in humans. *CPT Pharmacometrics Syst Pharmacol*. 2017 Jan 28. doi: 10.1002/psp4.12153.
- Thiel C, Cordes H, Fabbri L, Aschmann HE, Baier V, Smit I, Atkinson F, Blank LM, Kuepfer L. A comparative analysis of drug-induced hepatotoxicity in clinically relevant situations. *PLoS Comp. Biol.*, 2017.